# Tailored Triarylborane Polymers as Supported Catalysts and Luminescent Materials

*Huina Lin,[a] Shivani Patel,[a] and Frieder Jäkle [a]**

* *fjaekle@rutgers.edu*

[a] Department of Chemistry, Rutgers University-Newark, 73 Warren Street, Newark, NJ 07102, USA

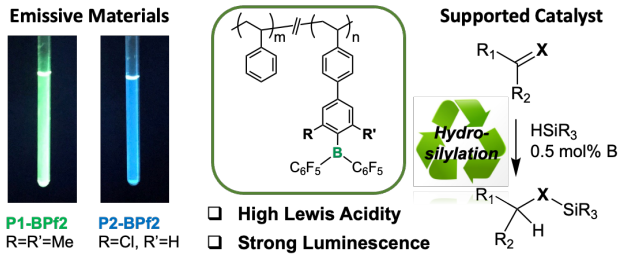


**Abstract.** Two novel luminescent triarylborane polymeric Lewis acids and the corresponding molecular model compounds were prepared, studies on their photophysical properties performed, and applications as supported catalysts in Lewis acid-catalyzed hydrosilylation reactions explored. Variations of the substituents in the *ortho*-position of a phenylene linker between the Lewis acidic borane and the polystyrene framework lead to steric and electronic fine-tuning while retaining the high Lewis acidity of the boron center. The polymeric Lewis acids serve as effective catalysts in the hydrosilylation of aldehyde, ketone, and imine compounds, and due to their distinct solubility

characteristics are readily amenable to recycling. In addition, as a result of the twisted biphenyl donor-π-acceptor structure, both the styrene copolymers and model compounds display strong luminescence in solution and the solid state, encompassing prompt and in the case of the chlorophenyl-linked derivative even longer-lived room temperature phosphorescence (RTP). Consistent with quantum chemical calculations, the greater donor strength of the 2,6-dimethylphenyl in comparison to the 2-chlorophenyl linker leads to a red-shifted emission, while the chloro substituent leads to a larger gap between singlet and triplet excited states. In the solid state, distinctly different emission properties are observed for the polymers in comparison to the molecular compounds due to the site isolation of the chromophores embedded in the polymer matrix.

## Introduction

Benefiting from a readily accessible low-lying vacant $p_z$ orbital on boron, triarylboranes serve important roles both as electron acceptors and as powerful Lewis acids.[1] Their electron-deficient character and desirable photophysical properties are exploited in applications ranging from nonlinear optics to organic light-emitting diodes, organic field-effect transistors, and organic photovoltaics.[2-3] The tunable Lewis acidity of triarylboranes is advantageous in anion sensing, catalysis and small molecule activation. Following the successful implementation of organoboranes in "frustrated Lewis pairs" (FLPs) chemistry by Stephan[4-5] they have been applied in numerous catalytic processes including hydrogenation, hydroamination, and $CO_2$ reduction.[6-8] The high Lewis acidity of organoboranes also facilitates catalytic hydrosilylation based on a weak Lewis acid (LA)-Lewis base (LB) interaction between boron and hydrosilanes.[9-12] In all these processes the use of organoboranes as organocatalysts avoids the need for transition metal complexes that are oftentimes expensive and/or toxic.

The attachment of borane moieties to polyolefins offers access to polymer-supported Lewis acids (PLAs, Figure 1), potentially providing an opportunity to take advantage of the reusability of the polymers and to achieve more sustainable catalytic processes.[13-16] On the other hand, organoborane-based fluorescent polymers are also promising as optoelectronic materials.[17-20] Polymers with tunable emission color, intensity, and delayed fluorescence characteristics are highly sought after for display applications.[21] In 2002, we first reported on the introduction of Lewis acidic boranes into the side chains of polystyrene via facile substituent exchange reactions on boron, leading to a family of well-defined PLAs (**A**).[22-23] Straightforward substituent exchange reactions also provided access to borane polymers with π-conjugated bithiophene, carbazole and fluorene pendent groups that are both Lewis acidic and strongly fluorescent (**B**).[24-27] These polymers were applied as ratiometric sensors for small anions such fluoride or cyanide. We later demonstrated the controlled polymerization of a dimesitylborane ($Mes_2B$)-substituted vinylbiphenyl monomer via reversible addition fragmentation chain transfer (RAFT) and discovered that a luminescent block copolymer with PNIPAM (**C**) can be used to detect fluoride anions in aqueous solution at a remarkably low level of less than 1 ppm.[28] More recently, researchers have explored Lewis acidic organoborane polymers as macromolecular building blocks for advanced supramolecular materials. For instance, Shaver and coworkers demonstrated that the addition of a small molecule, such as diethyl azodicarboxylate, can promote rapid and reversible network formation between Lewis acidic $Ph_2B$- (**D**) and Lewis basic $Mes_2P$-substituted polystyrenes.[29-30] In the absence of the additive, the LA and LB groups do not interact due to the large steric hindrance on the P sites, instead acting as FLPs. Dithienylborane-substituted polystyrenes (**E**) have also proven to be excellent building blocks for the formation of transient

polymer networks and recyclable elastomers via reversible formation of B-N classical Lewis pairs (CLPs).[31-32]

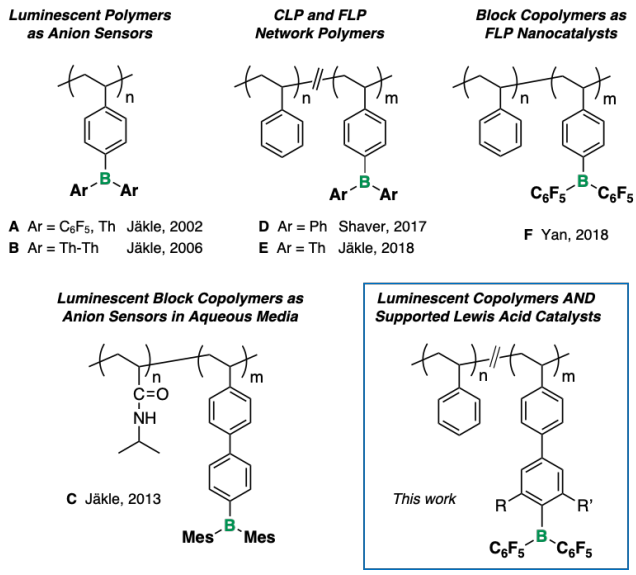


**Figure 1.** Examples of triarylborane Lewis acid-functionalized polymers and their applications

Although several semi-immobilized systems have been reported,[33-35] applications of soluble organoborane polymers in catalysis remain scarce. Recently, Yan and coworkers introduced a new $CO_2$-responsive system for the catalytic formylation of N-H bonds based on two complementary Lewis acidic organoborane (**F**) and Lewis basic organophosphine block copolymers. Interestingly, in their system $CO_2$ acts as a cross-linker that enables micelle formation as recyclable nanocatalysts.[36] However, one of the obstacles to broader implementation of polymer-supported borane LAs and FLPs is that sterically unprotected arylboranes, such as $Ph_3B$ or $PhB(C_6F_5)_2$, undergo gradual hydrolysis and are easily deactivated by Lewis base impurities or substrate functionalities that form strong Lewis pair complexes. The stability of organoboranes can be effectively enhanced by two strategies: (i) the introduction of bulky substituents around the boron

atom and (ii) the mitigation of the electron-deficiency at boron in that electron-withdrawing groups are used only to the extent necessary to achieve efficient catalysis. Recognizing these issues, Soos, Wildgoose, and Ashley tailored molecular organoborane LAs, optimizing the steric and electronic properties by judicial introduction of substituents ($CH_3$, $CF_3$, Cl) in *ortho*-position of the B-aryl substituents.[37-41]

In a first foray into tailor-made luminescent PLAs and FLPs that are more robust, yet highly active, we set out to prepare copolymers that feature an additional benzene ring between the borane functional group and the polymerizable styryl group. This allows us to stabilize the borane moiety with bulkier groups in *ortho*-position while also tuning the Lewis acidity. We designed two systems to match these requirements. The *ortho*-methyl groups in **P1** are expected to sterically retard the binding of Lewis bases (including water) to the Lewis acidic center; similarly, the introduction of a chlorine atom in *ortho* position in **P2** provides some steric hindrance, but also enhances the electron-deficient character. The attachment of these tailored triarylborane moieties to a polyolefin backbone offers access to new polymer-supported Lewis acids with potential for recyclability.[42-44] These polymers display intriguing luminescent properties that could not only prove advantageous for visual observation of the catalyst state (bound vs unbound)[45-46] but also enable applications as new materials in optoelectronic devices.

## Results and Discussion

**Synthesis of Copolymers and Molecular Model Systems.** Precursor **1** was prepared by lithiation of 5-bromo-2-iodo-1,3-dimethylbenzene followed by quenching with $Me_3SiOTf$ according to a method reported in the patent literature,[47] and a similar synthesis was developed for **2** starting from 4-bromo-2-chloro-1-iodobenzene. These silylated arenes were converted to monomers **M1** and

**M2** by Suzuki-Miyaura coupling with 4-vinylphenylboronic acid (Scheme 1). The monomers were purified by column chromatography on alumina using hexanes as the eluent, and **M2** was further recrystallized from MeOH. The products were isolated as white solids in 47% and 53% yield, respectively. Similarly, Suzuki-Miyaura coupling of **1** and **2** with 4-*tert*-butylphenylboronic acid gave the model compounds **Mod1-Si** and **Mod2-Si** as white solid in 44% and 55% yield. The monomers **M1** and **M2** were then copolymerized with styrene in a 1:5 molar ratio in anisole with 1,1'-azobisisobutyronitrile (AIBN) as the initiator. After 24 h at 110 ºC, $^{1}$H NMR analyses showed that the copolymers **P1-Si** and **P2-Si** contain ca. 18 and 13 mol% of –$SiMe_3$ pendant group respectively, which matches well the monomer feed ratio. GPC analyses in THF gave estimated molecular weights of $M_n$ = 18.8 kDa ($Đ$ = 1.65) for **P1-Si** and $M_n$ = 39.3 kDa ($Đ$ = 2.09) for **P2-Si** relative to narrow polystyrene standards.

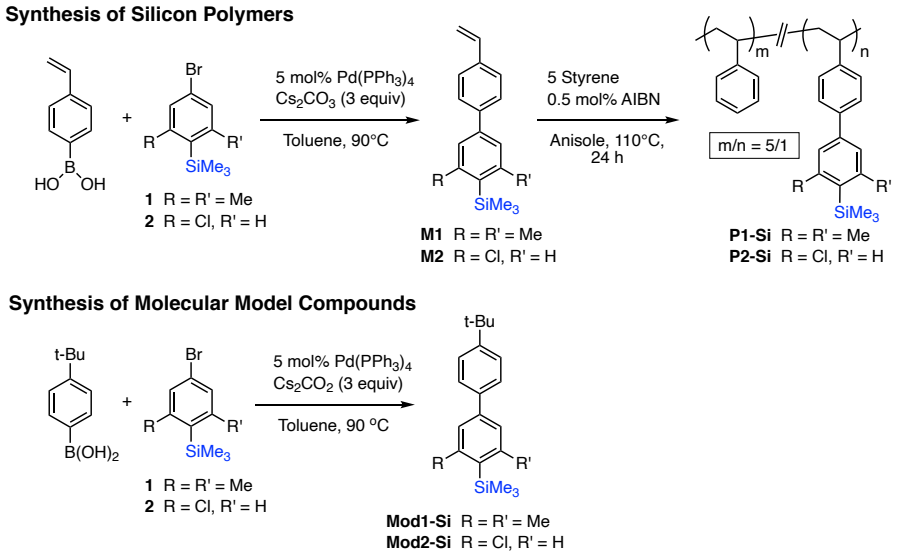


**Scheme 1.** Synthesis of Silane-functionalized Polymers and Model Compounds

The subsequent silicon-boron exchange to introduce the borane functional groups was first investigated on the molecular model compounds (Scheme 2). For **Mod1-Si**, the trimethylsilyl (TMS) groups were readily replaced with $BBr_2$ groups upon reaction with $BBr_3$ in a concentrated toluene solution at room temperature over 12 h. In contrast, the conversion of **Mod2-Si** to **Mod2-BBr2** required addition of an excess of $BBr_3$ (3 equiv.) and heating of the mixture to 80 ºC, because the inductive electron-withdrawing (–I) influence of the Cl substituent in *ortho* position slows down the electrophilic borylation. The disappearance of the TMS group in the $^{1}H$ NMR and the appearance of a signal at 63.0 and 57.4 ppm respectively in the $^{11}B$ NMR spectra both indicate that the Si-B exchange reactions proceeded successfully. As shown in Scheme 2, **Mod1-BPf2** and **Mod2-BPf2** were obtained by subsequent reaction with bis(pentafluorophenyl)zinc ($Zn(C_6F_5)_2$). Higher temperatures (80 ºC) and reaction times (48 hours) were required for the functionalization of **Mod1-BBr2** with $Zn(C_6F_5)_2$ (1.5 equivs.), while conversion of **Mod2-BBr2** to the product proceeded at room temperature over 24 hours with 1.05 equivs. of $Zn(C_6F_5)_2$. The structures of these model compounds were confirmed by $^{1}H$, $^{11}B$, $^{19}F$, and $^{13}C$ NMR spectroscopy (Figure S25-30 and Figure S36-41, SI). The $^{11}B$ NMR spectra showed broad downfield signals at 69.6 ppm (**Mod1-BPf2**) and 63.3 ppm (**Mod2-BPf2**), respectively, which are consistent with the expected chemical shifts of the tricoordinate arylboranes, and slightly downfield from those of the $BBr_2$-functionalized intermediates (63.0, 57.4 ppm). The typical patterns were observed in the $^{19}F$ NMR spectra with three separate signals for the *ortho*-, *meta*-, and *para*-F atoms on the $C_6F_5$ groups. A larger separation between the *para*- and *meta*-F atoms for **Mod1-BPf2** ($\Delta\delta$ = 15.4 ppm) in comparison to **Mod2-BPf2** ($\Delta\delta$ = 14.4 ppm) is consistent with the expected more electron-deficient character of **Mod2-BPf2**. The $^{1}H$ NMR spectra are also consistent with the expected structures. In addition, high-resolution MALDI-TOF MS data were acquired of the corresponding

fluoride anion complexes generated by addition of an excess of $[Bu_4N]F$ to solutions of the boranes in THF.

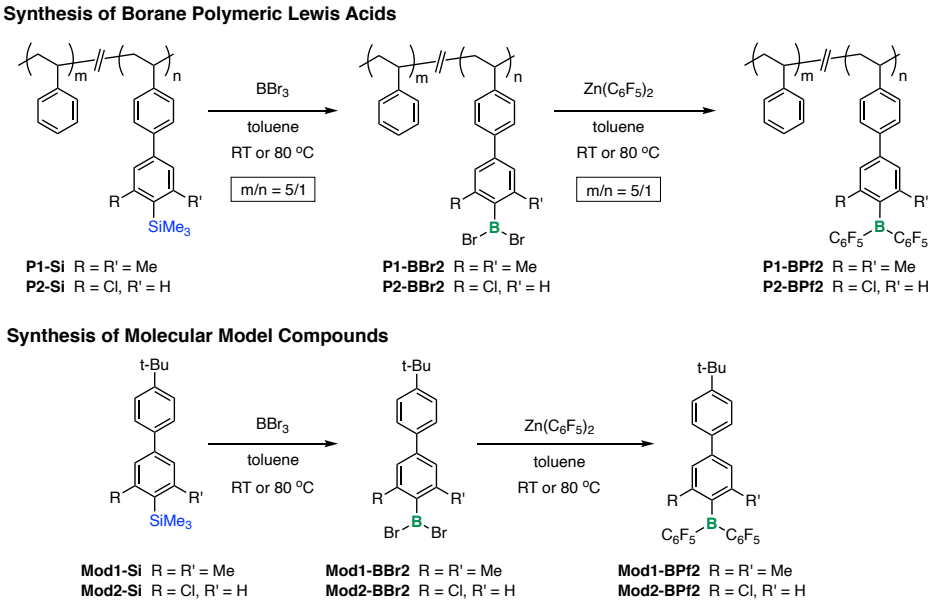


**Scheme 2.** Conversion to Arylborane-functionalized Polymers and Model Compounds

With this information in hand, we pursued the polymer modification of **P1-Si** and **P2-Si**. Using similar methods as for the model compounds the TMS groups were selectively exchanged with $BBr_3$ in toluene. As in the case of the model compound, for **P2-BBr2** an excess of $BBr_3$ and heating to 80 ºC were required to achieve close to quantitative borylation. The conversion to **P1-BBr2**/**P2-BBr2** was verified by the disappearance of the signal for the TMS groups in the $^1$H NMR spectra and the appearance of a signal at ~60 and ~55 ppm in the $^{11}$B NMR spectra respectively. For **P1-BBr2**, the signals for the methyl groups on the functional units shift from 2.52 to 2.39 ppm with only a small residual signal remaining for the precursor (< 5%) (Figure S9). The polymer **P1-BBr2** was used in situ for the subsequent arylation reaction, but **P2-BBr2** was first precipitated into anhydrous hexanes to remove the excess of $BBr_3$. The dibromoborylated polymers were converted

to the target polymers **P1-BPf2** and **P2-BPf2** by reaction with $Zn(C_6F_5)_2$. Under the conditions established for the model systems, **P1-BBr2** was reacted with 1.5 equivs. of $Zn(C_6F_5)_2$ at 80 ºC for 48 h and **P2-BBr2** with 1.05 equivs. of $Zn(C_6F_5)_2$ at room temperature for 24 h. The final products were isolated in 64 and 56% yield by repeated precipitation into hexanes and dried under high vacuum. The structures of the copolymers were confirmed by $^{1}H$, $^{11}B$ and $^{19}F$ NMR spectroscopy (Figure 2). The $^{19}F$ NMR spectra of **P1-BPf2** and **P2-BPf2** both show the typical set of three peaks for the *ortho*-, *meta*- and *para*-position fluorines on the $C_6F_5$ groups; the signals appear at chemical shifts that are similar to those of the model compounds but are slightly broadened. The $^{11}B$ NMR signals at 68.3 ppm and 62.9 ppm for **P1-BPf2** and **P2-BPf2**, respectively, are also consistent with those of the model compounds. In addition, a characteristic upfield shift of the methyl protons to 2.17 ppm for **P1-BPf2** from 2.52 ppm for **P1-SiMe3** is consistent with shifts seen for the model compounds. Importantly, for both **P1-BPf2** and **P2-BPf2** the integral ratios are in good agreement with those determined for the silylated precursors (Figures S11 and S18), suggesting a similar number of functional groups. The GPC traces of the triarylboranes substituted copolymers are very broad, indicating a small degree of crosslinking of the copolymers, likely due to the presence of a few $Ar_2B\text{-}O\text{-}BAr_2$ linkages as suggested by minor signals in the $^{11}B$ NMR spectra at ca. 40 ppm. The possible formation of B-OH/B-O-B species due to the presence of trace amounts of water during the synthesis or isolation processes was further examined by studying the stability of the compounds in wet $CDCl_3$ by $^{19}F$ and $^{11}B$ NMR spectroscopy in air. Gradual conversion to borinate species was observed over a period of four days for the model compounds (Figures S43-46, SI). For the polymers, precipitation occurred within 30 mins (Figures S47-49, SI), suggesting that even a small extent of hydrolysis results in an insoluble crosslinked material. Although the crosslinked

material is still catalytically active (*vide infra*), these findings suggest that, in the absence of Lewis base stabilization, the polymers are best handled in the absence of air and moisture.

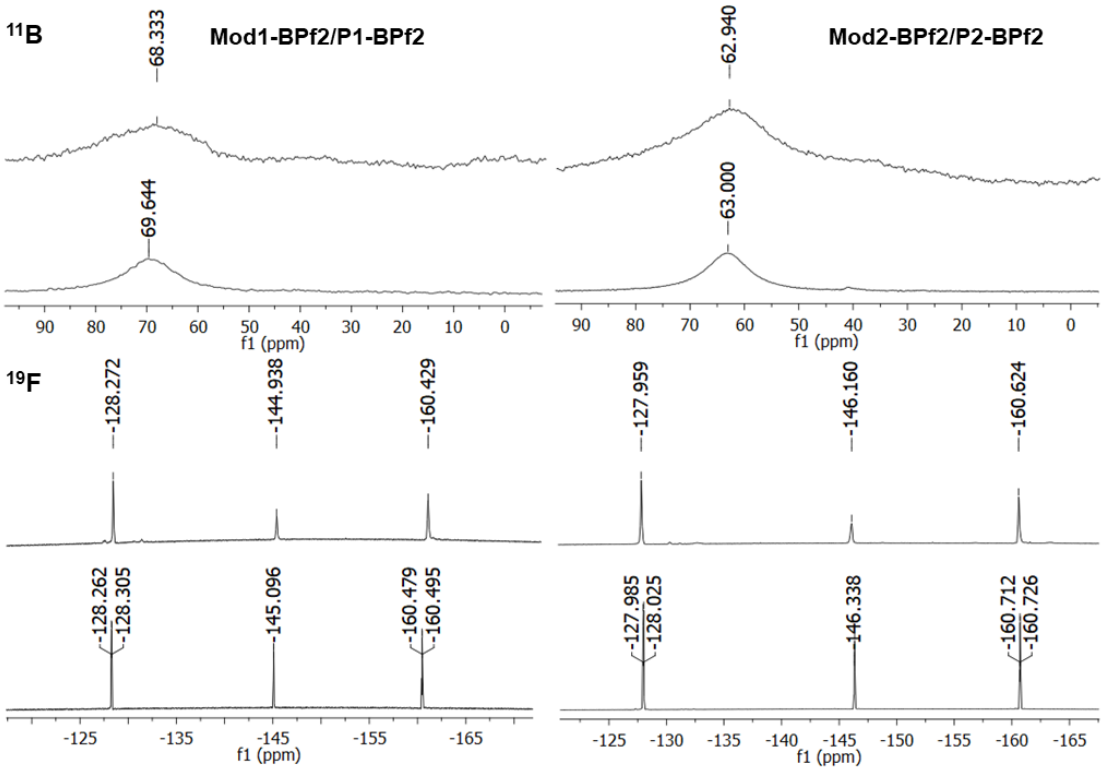


**Figure 2.** $^{19}F$ and $^{11}B$ NMR spectra of model compounds (bottom) and polymers (top) in $CDCl_3$.

**Determination of Lewis Acid Strength.** The relative Lewis acidity of the boron centers in the model compounds and polymers were estimated by treatment with triethylphosphine oxide ($Et_3PO$) according to the Gutmann-Beckett[48] method. The $^{31}P$ NMR shifts of the $Et_3PO$-borane complexes are summarized in Table 1 and compared to the adduct $(Et_3PO)$-$B(C_6F_5)_3$. All model compounds and copolymers are high Lewis acidic, having around 90% relative Lewis acid strength compared with $B(C_6F_5)_3$. **Mod2-BPf2** and **P2-BPf2** display relatively higher Lewis acidity than **Mod1-BPf2** and **P1-BPf2** due to the more electron-withdrawing chlorine substituent in *ortho*-position to the boron center. The complex formation for **Mod1-BPf2** and **P1-BPf2** proved to be dynamic at room temperature. Hence the studies were performed at low temperature (-20 ºC) where the equilibrium

between free acid and $Et_3PO$ is sufficiently slow to accurately determine the $^{31}P$ NMR chemical shift of the complex.

**Table 1.** Gutmann-Becket analysis of organoborane model compounds and polymers

| Compound | $\delta(^{31}P)$ for adduct (ppm) [a] | $\Delta\delta(^{31}P)$ [b] | Lewis acidity relative to $B(C_6F_5)_3$ (%) | Acceptor number (AN) [c] |
|---|---|---|---|---|
| **Mod1-BPf2** [d] | 74.0 | 21.3 | 90 | 72.9 |
| **P1-BPf2** [d] | 74.1 | 21.4 | 91 | 73.2 |
| **Mod2-BPf2** | 74.3 | 21.6 | 92 | 73.5 |
| **P2-BPf2** | 74.6 | 21.8 | 93 | 74.2 |
| **$B(C_6F_5)_3$** | 76.2 | 23.5 | 100 | 77.8 |

[a] $^{31}P$ NMR shifts are recorded in $CDCl_3$ relative to $H_3PO_4$ ($\delta$ = 0.00 ppm) as internal standard. [b] $\Delta\delta(^{31}P)$ = $\delta(^{31}P)$ adduct - 52.7 ppm. [c] Gutmann–Beckett method: $AN = 2.21\times(\delta^{31}_{LA\cdot Et3PO} - 41)$. [d] Data acquired at –20 ºC.

**Applications as Catalysts in Hydrosilylation Reactions.** The observed high Lewis acidity prompted us to explore applications in the Lewis acid catalyzed hydrosilylation of unsaturated organic substrates. The objective of these investigations was to test the capacity of these novel Lewis acids as recyclable catalysts. To explore the feasibility, we initially tested the borane model compounds in the catalyzed hydrosilylation of benzaldehyde (**1a**), acetophenone (**1b**), N-benzylideneaniline (**1c**), and styrene (**1d**). When using 10 mol% of the model compounds as catalysts, quantitative conversion of **1a** was achieved within 10 min (Table 2, entry 1, 2), demonstrating the high reactivity of these Lewis acids. This result suggested that even at much

lower catalyst loading the reactivity in the catalytic hydrosilylation reaction may be retained. Gratifyingly, both **Mod1BPf2** and **Mod2-BPf2** were found to promote carbonyl hydrosilylation with 0.5 mol% model catalysts loading, reaching high conversions within short reaction time (Table 2, entry 3-6). When directly comparing their catalytic performance, **Mod2-BPf2** showed relatively higher efficiency. This efficiency difference becomes more pronounced in the hydrosilylation of imine **1c** (Table 2, entry 7, 8). While 2 mol% of **Mod1-BPf2** resulted in 69% conversion at 50 ºC after 48 h, the more Lewis acidic **Mod2-BPf2** gave full conversion at ambient temperature over 24 h. Finally, the hydrosilylation of styrene was probed. Even with 10 mol% **Mod1-BPf2** no conversion of the relatively less nucleophilic styrene could be achieved over 48 hours at 60 ºC. In contrast, when applying 10 mol% of **Mod2-BPf2** 29% conversion was reached at 30 ºC after 48 hours. In all cases the structure of hydrosilylated products was confirmed by comparison with $^1$H NMR data reported in the literature. For the hydrosilylation of styrene only one isomer was detected, (2-phenylethyl)trimethylsilane, consistent with the results reported when using $B(C_6F_5)_3$ as the catalyst.[7b]

**Table 2.** Investigation of Lewis acids in catalytic hydrosilylation of selected substrates.[a]

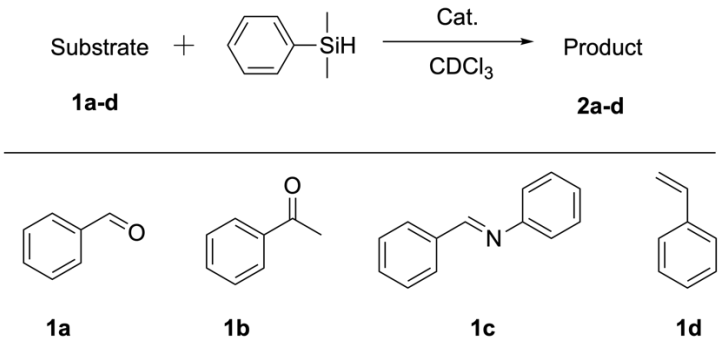


| entry | substrate | catalyst | cat. loading (mol%) | temp / time (ºC / h) | conversion (%) |
|---|---|---|---|---|---|

| | | | | | |
|---|---|---|---|---|---|
| 1 | **1a** | **Mod1-BPf2** | 10 | 25 / 10 min | 100 |
| 2 | **1a** | **Mod2-BPf2** | 10 | 25 / 10 min | 100 |
| 3 | **1a** | **Mod1-BPf2** | 0.5 | 25 / 0.5 | 95 |
| 4 | **1a** | **Mod2-BPf2** | 0.5 | 25 / 0.5 | 100 |
| 5 | **1b** | **Mod1-BPf2** | 0.5 | 25 / 2.5 | 100 |
| 6 | **1b** | **Mod2-BPf2** | 0.5 | 25 / 2.5 | 100 |
| 7 | **1c** | **Mod1-BPf2** | 2 | 50 / 48 | 69 |
| 8 | **1c** | **Mod2-BPf2** | 0.5 | 25 / 24 | 96 |
| 9 | **1d** | **Mod1-BPf2** | 10 | 60 / 48 | 0 |
| 10 | **1d** | **Mod2-BPf2** | 10 | 30 / 48 | 29 |
| 11 | **1a** | **P1-BPf2** | 0.5 [b] | 25 / 0.5 | 71 |
| 12 | **1a** | **P2-BPf2** | 0.5 [b] | 25 / 0.5 | 100 |
| 13 | **1b** | **P1-BPf2** | 0.5 [b] | 25 / 2.5 | 100 |
| 14 | **1b** | **P2-BPf2** | 0.5 [b] | 25 / 2.5 | 100 |
| 15 | **1c** | **P1-BPf2** | 0.5 [b] | 25 / 24 | 32 |
| 16 | **1c** | **P2-BPf2** | 0.5 [b] | 25 / 24 | 100 |

[a] All reactions were performed inside a glovebox at 0.2 M (2 mol% or 10 mol% catalyst) or 0.8 M (0.5 mol% catalyst) substrate concentration of **1**, 1.2 equiv. of dimethylphenylsilane, and the noted mol% of catalyst in $CDCl_3$ (0.5 mL). [b] Mol% of borane Lewis acid functional groups.

Having identified the catalytic efficiency of the borane model systems, we next focused on exploring the polymeric Lewis acids in the hydrosilylation of **1a**, **1b** and **1c**. When keeping the loading of the active borane moieties in the polymer constant, **P1-BPf2** and **P2-BPf2** display similar catalytic efficiency as the corresponding model compounds (Table 2, entry 11-16), with

superior results achieved for the polymeric Lewis acid **P2-BPf2**. This suggests that the catalytic sites in the polymer are readily accessible resulting in quantitative conversion of benzaldehyde, acetophenone, and benzylideneaniline at only 0.5 mol% of boron sites. While the superior catalytic performance of **P2-BPf2** is attributed primarily to the higher Lewis acidity, a more rapid degradation of **P1-BPf2** could also play a role. Whereas a homogenous solution of **P2-BPf2** formed with most substrates, swollen particles of **P1-BPf2** were found during the hydrosilylation reactions indicative of more pronounced polymer crosslinking. Using the more active catalyst, **P2-BPf2**, we examined additional substrates, including aldehydes with strongly electron-donating and electron-withdrawing groups attached to the phenyl ring of benzaldehyde (Figure S55, SI). Both electron-rich and electron-deficient benzaldehydes showed high conversion. A benzaldehyde with electron-donating methoxy groups in 3,5-position of the phenyl ring was quantitatively converted within 30 mins, whereas an electron-withdrawing nitro group in 4-position resulted in just slightly slower conversion (96% at 30 mins, 100 % after 24 h). In contrast, 4-dimethylaminobenzaldehyde gave only 3% conversion at 30 mins and 80% after 24 h. The lower reactivity could be due to the Lewis basic properties of the dimethylamino groups binding to reactive intermediates. The more hindered benzophenone was tested as well, giving quantitative conversion in only 30 mins. An important aspect is the potential reusability of the polymeric Lewis acids. Using **P2-BPf2** as the more active and more robust catalyst, we found that by simply removing the solvents under vacuum and washing the product mixture with hexanes the polymeric catalyst could be separated from the final product (confirmed by $^{1}$H NMR) and the catalytic processes repeated for at least 5 times. The catalytic activity towards benzaldehyde was retained, achieving 95% conversion in the fifth cycle (Figure S56, SI). This qualitative result suggests that, due to the high Lewis acidity and

low solubility in non-polar solvents, polymers such as show promise as reusable Lewis acid catalysts for hydrosilylation reactions.

**Photophysical Properties.** During the course of our studies we discovered that both the organoborane model compounds and the copolymers are strongly luminescent in solution. This suggests potential utility also as materials for optoelectronic device or imaging applications. Since the first demonstration by Shirota and coworkers that bithiophene or terthiophene with $Mes_2B$ substituents can be used as efficient electron-transporting materials in OLEDs,[49] many different luminescent materials based on tricoordinate organoboranes have been designed.[2-3] More recently, researchers have discovered organoborane donor-acceptor systems that exhibit highly effective thermally activated delayed fluorescence (TADF) and even room temperature phosphorescence (RTP).[50-54] Relevant to our studies is the work by Zhao and coworkers who reported that triarylborane-triarylamine systems with [2.2]paracyclophane, twisted biphenyl or binaphthyl backbones display charge transfer emissions that, depending on the system, are temperature-dependent, circularly polarized, or exhibit TADF characteristics.[55-57] Of note is also work by Thilagar and coworker who designed simple structures exhibiting TADF, which encompass tridurylboranes with $NR_2$ (R = H, Me) donor moieties.[52] In all these compounds, the spatial separation of the donor-centered HOMO and acceptor-centered LUMO plays an important role in enabling the TADF behavior.[58] A recent study by Marder also reveals the observation RTP of arylboranes, even in the absence of strong electron donor groups on the substituents.[54] While most studies have focused on $Mes_2B$ groups as acceptors, Marder and coworkers found that the much enhanced acceptor strength of $(FMes)_2B$ (FMes = 2,4,6-tris(trifluoromethyl)phenyl) derivatives can be beneficial for optoelectronic application.[55,59] These findings prompted us to investigate the photophysical properties of our polymers and model compounds in more detail.

As seen in Table 3, the absorption and emission data for the copolymers **P1/P2-BPf2** closely track those of the molecular model compounds **Mod1/Mod2-BPf2**. This is expected considering that the functional group loading for the polymers is about 15%, thus spacing out the chromophores. The UV-visible absorption spectra of **Mod1-BPf2** and **Mod2-BPf2** in DCM show maxima at 386 and 363 nm, respectively (Figure 3). The absorptions for **Mod1**/**P1-BPf2** are redshifted relative to those of **Mod2**/**P2-BPf2**, likely due to elevation of the HOMO in the presence of the more electron-rich dimethylphenyl compared to the chlorophenyl group. The presence of a second band at around 260–270 nm for all compounds may indicate additional transitions that involve predominantly orbitals localized on the *para*-substituted phenyl ring that is common to both systems. In DCM solution, **Mod1**/**P1-BPf2** give rise to green emissions with maxima at 538 / 543 nm, while **Mod2**/**P2-BPf2** are blue-emissive with maxima at 483 / 490 nm. The fluorescence quantum yields of **Mod1**/**P1-BPf2** ($\Phi_{FL}$ = 0.34 / 0.31) are higher than those of **Mod2**/**P2-BPf2** ($\Phi_{FL}$ = 0.14 / 0.22), and the fluorescence lifetimes measured for **Mod1**/**P1-BPf2** ($\tau_{FL}$ = 35.6 / 34.6 ns) are significantly longer than those of **Mod2**/**P2-BPf2** ($\tau_{FL}$ = 6.9 / 8.4 ns, averaged for two components). From the $\tau_{FL}$ and $\Phi_{FL}$ values, the radiative ($k_r$) and nonradiative ($k_{nr}$) decay rate constants were calculated. **Mod2**/**P2-BPf2** show relatively larger $k_r$ and $k_{nr}$ values than **Mod1**/**P1-BPf2**. The only slightly larger $k_r$ values but significantly larger $k_{nr}$ values for **Mod2**/**P2-BPf2** lead to the observation of lower quantum yields for the chlorinated derivatives. A possible explanation is that intersystem crossing (ISC) is facilitated by the chlorine heavy atom effect. The small $k_r$ values, together with the large Stokes shifts, may also suggest a twisted excited state structure for these compounds.[55-56] The excited state structure of **Mod1-BPf2** is expected to be more distorted compared to that of **Mod2-BPf2**, because the *ortho*-methyl groups are sitting below and above the boron center, generating more steric hindrance. Considering the likely role of intramolecular

charge transfer (ICT) in the excited state, we also investigated the effects of changes in solvent polarity on the absorption and emission spectra. These studies were performed on the model compounds, because the range of suitable solvents is larger. The data are illustrated in Figure S57 and summarized in Table S1 (SI). While the absorption spectra are only slightly dependent on solvent polarity, the emission spectra exhibit a distinct positive solvatochromism. Upon changing the solvent from hexane to DCM, the emission maximum shifted from 469 to 538 nm for **Mod1-BPf2** and from 413 to 483 nm for **Mod2-BPf2**, indicative of a more polarized first excited state in comparison to the ground state.

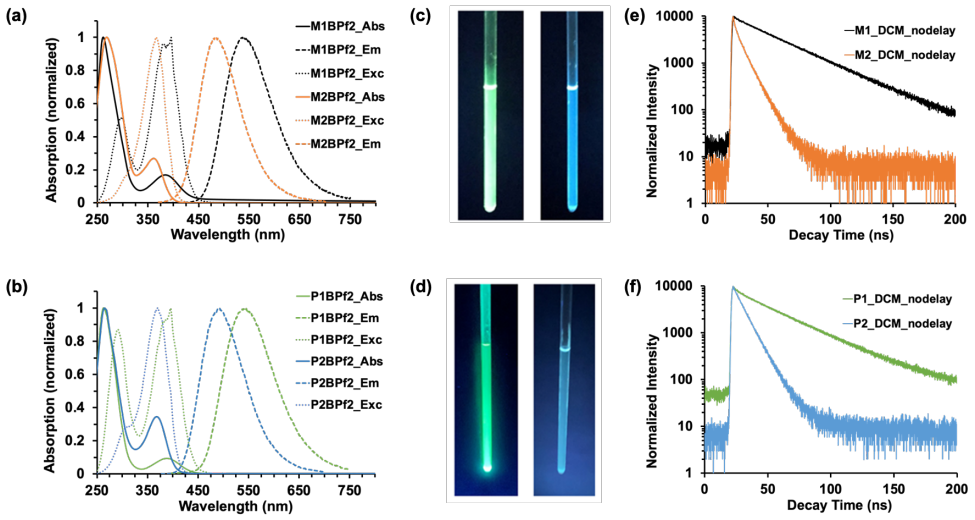


**Figure 3.** UV-vis absorption (Abs), excitation (Exc) and emission (Em) spectra of borane model compounds (a) and polymers (b) in DCM solution. Photographs of solutions of (c) **Mod1-BPf2** (left) / **Mod2-BPf2** (right) and (d) **P1-BPf2** (left) / **P2-BPf2** (right) in $CDCl_3$ irradiated with a handheld UV lamp (254 nm). Prompt fluorescence emission decay curves of (e) **Mod1/Mod2-BPf2** and (f) **P1/P2-BPf2** in DCM solution.

**Table 3.** Comparison of Photophysical Data of Model Compounds and Polymers

| Compound | $\lambda_{Abs}$ [a] (nm) | $\lambda_{Exc}$ [b] (nm) | $\lambda_{FL}$ [a] (nm) | *Stokes shift* ($cm^{-1}$) | $\tau_{FL}$ [d] (ns) | $\Phi_{FL}$ [e] | $k_r/k_{nr}$ [f] ($10^7$ $s^{-1}$) |
|---|---|---|---|---|---|---|---|
| **Mod1-BPf2** | 386, 260 | 392, 300 | 538 | 7300 | $\tau_1$ = 35.6, (100%) $\chi^2$ = 1.28 | 0.34 | 0.95/1.8 |
| **P1-BPf2** | 388, 263 | 389, 293 | 543 | 7300 | $\tau_1$ = 34.6, (100%) $\chi^2$ = 1.26 | 0.31 0.11 [h] | 0.89/2.0 |
| **Mod2-BPf2** | 363, 270 | 369, 302 | 483 | 6800 | $\tau_1$ = 1.7 (20%) $\tau_2$ = 8.2 (80%) $\chi^2$ = 1.59 [g] | 0.14 | 2.0/12.4 |
| **P2-BPf2** | 367, 265 | 369, 305 | 490 | 6800 | $\tau_1$ = 7.9 (95%) $\tau_2$ = 18.6 (5%) $\chi^2$ = 1.44 | 0.22 0.05 [h] | 2.6/9.3 |

[a] In DCM solution. [b] Excitation data for maximum emission. [c] Excited at the lowest energy absorption maxima. [d] Excited with a nanoLED at 390 nm. [e] Absolute quantum yield determined using an integrating sphere. [f] Radiative ($k_r$) and nonradiative ($k_{nr}$) decay rate constants are calculated using the equations $k_r = \Phi/\tau$, $k_{nr} = (1 - \Phi)/\tau$. [g] For triple-exponential fit: **Mod2-BPf2**: $\tau_1$ = 1.2 ns (14 %), $\tau_2$ = 6.7 ns (64 %); $\tau_3$ = 11.2 ns (22 %); $\chi^2$ = 1.42. [h] Quantum yield for solid samples.

Time-gated spectroscopic studies were carried out on the model compounds and the copolymers both at room temperature and at 77 K, revealing the presence of additional slower emission pathways (Table S2). The spectral data acquired in the solid state for **P1-BPf2** and **P2-BPf2** were qualitatively very similar to data in toluene for either the model systems or the polymer (Figure S59 and S60). This is expected considering that the loading of the chromophore is low (ca. 15%) and thus the chromophores are molecularly dispersed in the polymer matrix. On the other

hand, more complex data are seen for the model compounds in the solid state at 77 K, presumably due to intermolecular interactions between chromophores (Figure S61 and S62). Below, the data for the copolymers are discussed in detail, whereas corresponding data for the model compounds are summarized in the SI. As seen in Figure 4, at room temperature the prompt and gated emission spectra of **P1-BPf2** are overall similar, although a slight hypsochromic shift from 511 to 497 nm and narrowing of the band is observed with a 1 ms delay. When acquiring the data at 77 K, a structured lower energy band was observed with a maximum at 535 nm ($\tau_P$ = 623 ms) that is not seen at RT and can be attributed to phosphorescence from a triplet excited state. A different scenario is encountered for polymer **P2-BPf2**. Even at RT, a 1 ms delay leads to dual emission with a shoulder band at ca. 460 nm that is accompanied by a more intense band at a longer wavelength of 518 nm with a much longer lifetime of $\tau_1$ = 62.6 ms (58%), $\tau_2$ = 17.9 ms (42%). When acquiring the data at 77 K only the longer wavelength band at 518 nm is observed with a lifetime of $\tau_1$ = 148.6 ms (69%), $\tau_2$ = 373.3 ms (31%), consistent with phosphorescent decay from a triplet excited state. These results indicate that at room temperature phosphorescence is competing with fluorescence for **P2-BPf2**. The different behavior of **P2-BPf2** in comparison to **P1-BPf2** may be in part due to the heavy atom effect of the Cl substituent, favoring ISC, while the relatively large gap between the first excited singlet and triplet states of $\Delta E_{ST}$ = 0.37 eV makes reverse intersystem crossing (RISC) from the triplet ($T_1$) back to the first singlet excited state ($S_1$) unfavorable.

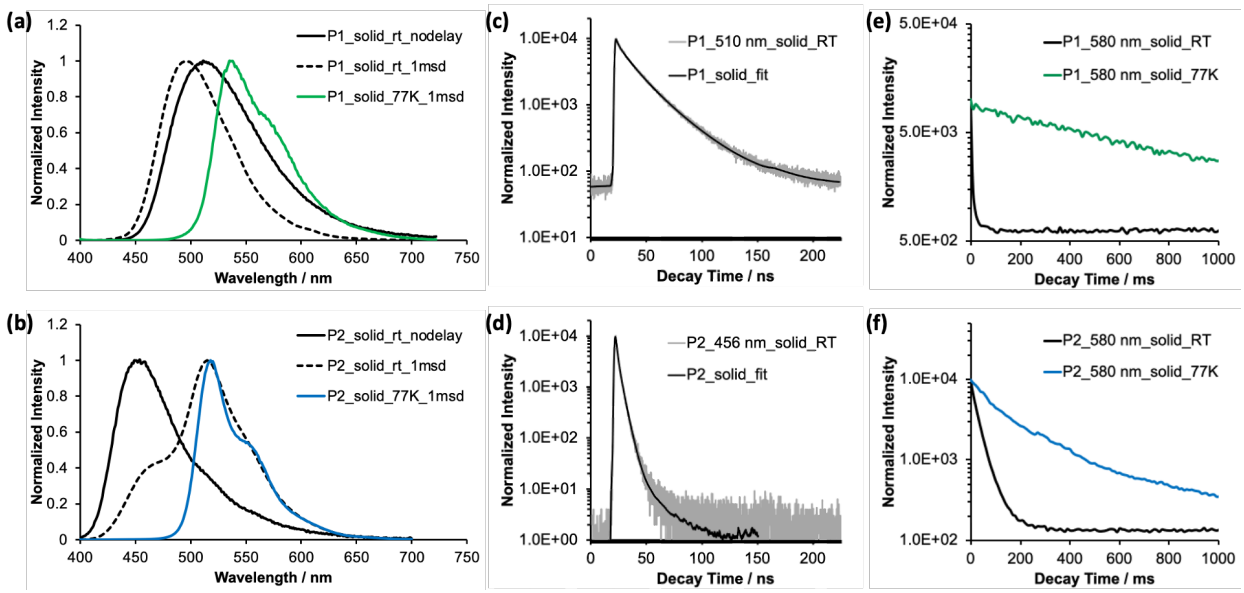


**Figure 4.** (a, b) Prompt and delayed (1 ms delay) emission spectral data of polymers **P1-BPf2** (top) and **P2-BPf2** (bottom) at RT and 77 K in the solid state. (c, d) Prompt decay of polymers **P1-BPf2** (top) and **P2-BPf2** (bottom) at RT in the solid state monitored monitored at 510 and 456 nm respectively. (e, f) Phosphorescent decay of polymers **P1-BPf2** (top) and **P2-BPf2** (bottom) at RT and 77 K in the solid state monitored at 580 nm.

**Theoretical calculations.** To shed further light into the electronic structures and the orbitals involved in the electronic transitions computational studies were performed on the model systems at the b3lyp/6-31g(d) level of theory using the polarizable continuum model (PCM) for solvation in DCM. As seen in Figure 5, for **Mod1-BPf2** and **Mod2-BPf2**, the HOMO is localized mainly on the 4-(*tert*-butyl)-1,1'-biphenyl groups, with a small contribution from the nominally empty p-orbital on the boron atom. The LUMO is localized primarily on the boryl group, with some contribution from the boron-bound phenyl ring. The HOMO and LUMO energy levels are -5.90 and -2.53 eV for **Mod1-BPf2**, but significantly lower at -6.25 and -2.65 eV for **Mod2-BPf2**. This difference is consistent with cyclic voltammetry data for the reduction of **Mod1-BPf2** (onset at -

1.68 V vs. Fc) and **Mod2-BPf2** (onset at -1.19 vs Fc) (Figure S65). These values are consistent with reported data[60] for structurally related compounds (-1.72 V for $MesB(C_6F_5)_2$ and -1.17 V for $B(C_6F_5)_3$). The corresponding LUMO energy levels at -3.12 eV and -3.61 eV, estimated using the formula $E_{LUMO} = –4.8 - E_{red}$ (eV), even are even lower than those determined computationally.

TD-DFT calculations (rcam-b3lyp/6-31g(d)) suggest a small oscillator strength of $f$ = 0.0992 for the $S_0$-$S_1$ transition of **Mod1-BPf2**, in good agreement with the weak intensity of the lowest energy absorption. However, a much larger $f$ = 0.6619 was found for **Mod2-BPf2**, which clearly overestimates the intensity of the experimental lowest-energy absorption of the latter (Table 4). To address this apparent discrepancy, we carried out a single-point TD-DFT calculation for **Mod2-BPf2** using the optimized **Mod1-BPf2** geometry, but with the methyl groups replaced for –H and –Cl at a distance of 1.771 Å. Using this geometry, an oscillator strength of $f$ = 0.1300 for the lowest energy absorption of **Mod2-BPf2** was found, which is in good agreement with the experimental data (Table S3, SI). The computed excitation wavelengths for the $S_0$-$S_1$ transition are 353 nm (**Mod1-BPf2**) and 326 nm (**Mod2-BPf2**; 324 nm for the modified structure using the geometry of **Mod1-BPf2**). These values are reasonably consistent with the experimental lowest-energy absorption maxima.[61] The relatively larger HOMO-LUMO energy gap for **Mod2-BPf2** correlates well with the shorter wavelength absorption maxima of **Mod2-BPf2** in comparison to **Mod1-BPf2**. For both, the HOMO and LUMO predominantly contribute to the excitation to $S_1$, suggesting significant intramolecular charge transfer (ICT) character for this process. This supports the experimentally observed emission solvatochromism of these compounds. The simulated fluorescence emission data based on TD-DFT optimizations of the $S_1$ states (Table 4) are again slightly higher in energy,[61] but overall consistent with the experimental data.

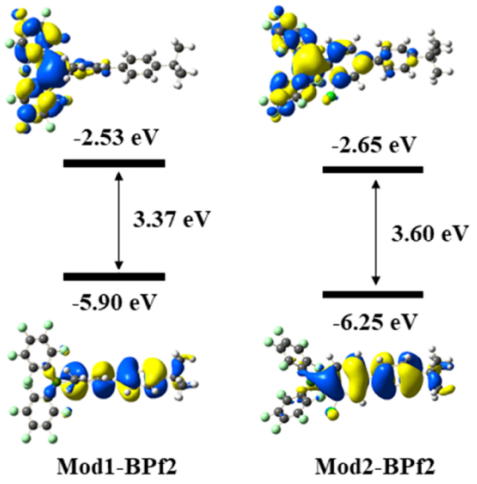


**Figure 5.** DFT calculated frontier orbitals for **Mod1-BPf2** and **Mod2BPf2** (rb3lyp/6-31g(d), DCM solvation model, isovalue = 0.02)

**Table 4.** TD-DFT calculated photophysical data for **Mod1-BPf2** and **Mod2-BPf2** (rcam-b3lyp/6-31g(d), DCM solvation model)

| | Transition (*f*) | $E_{ex}$ [a] (eV) | $\lambda$ [a] (nm) | Dominant components [b] (%) |
|---|---|---|---|---|
| | | **Absorption** | | |
| **Mod1-BPf2** | $S_0 \rightarrow S_1$ (0.0992) | 3.51 (3.21) | 353 (386) | HOMO-5 → LUMO (18)<br>HOMO → LUMO (77) |
| **Mod2-BPf2** | $S_0 \rightarrow S_1$ (0.6619) | 3.81 (3.41) | 326 (363) | HOMO → LUMO (74) |
| | | **Emission**[c] | | |
| **Mod1-BPf2** | $S_1 \rightarrow S_0$ (0.0126) | 2.94 (2.30) | 421 (538) | H-SOMO-4 → L-SOMO (10)<br>H-SOMO → L-SOMO (84) |
| **Mod2-BPf2** | $S_1 \rightarrow S_0$ (0.0406) | 3.27 (2.57) | 379 (483) | H-SOMO → L-SOMO (84) |

[a] Values in parentheses are experimental longest-wavelength absorption or emission maxima in DCM. [b] Components with greater than 10% contribution shown. Percentage contribution approximated by $2 \times (c_i)^2$

×100%, where $c_i$ is the coefficient for the particular 'orbital rotation'. [c] Taken as the reverse of excitation to $S_1$ from $S_0$ at the optimized $S_1$ geometry.

Finally, an investigation of the first triplet excited state ($T_1$) was attempted for both model compounds using the ub3lyp functional with a 6-31g(d) basis set and DCM solvation. The estimated difference in vertical transition energies $\Delta E_{ST}$ between the singlet ($S_1$) and triplet ($T_1$) excited states is computed to be much smaller for **Mod1-BPf2** (0.089 eV) in comparison to **Mod2-BPf2** (0.242 eV). The results agree well with experimental data for the copolymers that were derived from low temperature photophysical studies discussed earlier (Figure S64).

## Conclusions

To summarize, one part of our investigations was dedicated to the design of new polymeric Lewis acids for catalytic hydrosilylation. Two novel copolymers and their corresponding model compounds have been developed and employed as catalysts for the hydrosilylation of C=O or C=N bonds. These systems encompass either two *ortho*-methyl or an *ortho*-chlorine substituent to provide steric and electronic fine-tuning of the Lewis acidic component. In this way, the high Lewis acidity required for efficient catalysis is maintained while enhancing the stability and expanding the substrate scope. Superior catalytic properties were found for the more electron-deficient and more robust polymer **P2-BPf2**. Due to the distinct solubility characteristics, the polymer-supported Lewis acid **P2-BPf2** is amenable to recycling, as the polymer can be recovered by simple washing with hexanes.

Another part of the present work comprised an investigation of the electronic structure and photophysical properties through a combination of experimental and computational studies. We

found that the photophysical properties also vary with the substituents in the *ortho*-positions. The methyl groups in the bridge render **Mod1**/**P1-BPf2** more electron-rich than **Mod2**/**P2-BPf2** with a chlorine substituent. As a result, in DCM solution **Mod1**/**P1-BPf2** show green emission, while **Mod2**/**P2-BPf2** are blue-emissive. In addition, **Mod1**/**P1-BPf2** display longer fluorescence lifetimes and higher quantum yields than **Mod2**/**P2-BPf2**. Using time-gated spectroscopy we found evidence of long-lived room temperature phosphorescence for **P2-BPf2**. This discovery represents the first observation of RTP in tricoordinate organoborane polymers, suggesting much promise for further exploration. Measurements at 77 K substantiated the phosphorescent decay and provided an experimental estimate of $\Delta E_{ST}$ = 0.21 for **P1-BPf2** and $\Delta E_{ST}$ = 0.37 eV for **P1-BPf2**. The difference in $\Delta E_{ST}$ was further confirmed by TD-DFT calculations on molecular model systems.

Overall, our results indicate the strong potential of structurally fine-tuned polymer-supported Lewis acids as catalysts in the hydrosilylation of C=X bonds (X = O, N) with favorable recyclability, whereas the intriguing emissive properties suggest potential utility as luminescent materials.

## Experimental Section

Toluene and hexanes were purified using a solvent purification system (Innovative Technologies) and stored over Na/K alloy. Diethyl ether was distilled from Na/benzophenone; anisole and all chlorinated solvents were distilled from $CaH_2$. Azobisisobutyronitrile (AIBN) initiator was recrystallized in methanol. All other chemicals were purchased from commercial sources and directly used without further purification. All oxygen- and moisture-sensitive manipulations were

carried out under an inert atmosphere using either standard Schlenk techniques or a glove box. Reactions involving $BBr_3$ were conducted in Teflon-stoppered Schlenk tubes, avoiding the use of silicone grease.

NMR data were acquired at 25 ºC. 500.0 MHz $^{1}H$, 160.4 MHz $^{11}B$, and 470.3 MHz $^{19}F$ NMR data were recorded on a 500 MHz Bruker AVANCE spectrometer; 500.2 MHz $^{1}H$ and 125.8 MHz $^{13}C$ NMR data on a 500 MHz Bruker Auto AVANCE spectrometer; and 599.7 MHz $^{1}H$, 150.8 MHz $^{13}C$ and 192.4 MHz $^{11}B$ NMR data on a Varian INOVA 600 spectrometer. $^{11}B$ NMR spectra were acquired with boron-free quartz NMR tubes either on the Varian INOVA 600 with a boron-free 5 mm dual broadband gradient probe (Nalorac, Varian Inc., Martinez, CA) or the 500 MHz Bruker Auto Avance with a 5mm PH SEX 500S1 11B-H/F-D probe. $^{1}H$ and $^{13}C$ NMR spectra were referenced internally to solvent signals ($CDCl_3$: 7.26 ppm for $^{1}H$ NMR, 77.16 ppm for $^{13}C$ NMR) and all other NMR spectra externally to $SiMe_4$ (0 ppm).

UV-visible absorption data were acquired on a Varian Cary 5000 UV-Vis/NIR spectrophotometer or a Cary 60 UV-Vis spectrophotometer. The fluorescence data and lifetimes were measured using a Horiba Fluorolog-3 spectrofluorometer equipped with a 390 nm nanoLED and a FluoroHub R-928 detector. The delayed emission lifetimes were measured using a FL-1040A phosphorimeter incorporated into the Fluorolog setup. The excitation source was a pulsed xenon flash lamp, the full-width half-maximum of each pulse is 3 μs. A delay of 0.1 ms was used to ensure full decay of the prompt fluorescent response and the Xe lamp output. Absolute quantum yields ($\Phi_F$) were measured on the HORIBA Fluorolog-3 using a pre-calibrated Quanta-φ integrating sphere. Light from the sample compartment is directed into the sphere via a fiber-optic cable and an F-3000 Fiber-Optic Adapter, and then returned to the sample compartment (and to the emission monochromator) via a second fiber-optic cable and an F-3000 Fiber-Optic Adapter.

Measurements at 77 K were performed using an Fl-1013 liquid nitrogen dewar assembly while purging the sample compartment with dry nitrogen.

GC-MS data were acquired on an Agilent HP6890 GC System with an HP-5MS 5% phenyl methyl siloxane column and Agilent 5973A inert XL EI/CI MSD using helium as the carrier gas at a flow rate of 1 mL/min. The initial oven temperature was 50 °C, after holding for 3 mins the temperature was increased with a 10 °C/min ramp to a final temperature of 220 °C, then held at 220 °C for 15 min (splitless mode of injection, total run time of 22.0 min). MALDI-TOF MS measurements were performed on a Bruker Ultraflextreme in reflection mode with delayed extraction. Red phosphorus was used for calibration.

GPC-RI analyses were performed in THF (1.0 mL/min, 35 °C) using a Viscotek GPCmax with a VE 2001 GPC solvent/sample module, a 2600 UV-PDA detector, and a TDA 305 triple detector array. A set of two columns consisting of one PLgel 5 mm mixed-D and one PLgel 5 mm mixed-C column was used for separation and ten narrow polystyrene standards (580 Da – 364000 Da, Polymer Laboratories, Varian Inc.) for calibration.

All calculations (DFT and TD-DFT) were carried out with the program package Gaussian 16 (Rev. B.01 or Rev. D.01) and were performed on a parallel cluster system. The input files were generated from Chem3D and pre-optimized in Spartan '08 V 1.2.0. Ground state geometries were then optimized in Gaussian 16 using the hybrid density functional b3lyp with a 6-31g(d) basis set. Frequency calculations were performed to confirm the presence of local minima (only positive frequencies). Vertical excitations were calculated by TD-DFT methods at the rcam-b3lyp/6-31g(d) and rb3lyp/6-31g(d) level. First triplet excited state geometries were optimized by DFT methods at the ub3lyp/6-31g(d) level and first singlet excited state geometries were optimized by TD-DFT

methods at the b3lyp/6-31g(d) level. All calculations were performed using the polarizable continuum model (PCM) for solvation in DCM.

Details of the synthesis and characterization of the monomers and model compounds are provided in the Supporting Information.

**Synthesis of Poly((3,5-dimethyl-4'-vinyl-[1,1'-biphenyl]-4-yl)trimethylsilane)-co-Polystyrene (P1-Si).** In a glovebox, monomer **M1** (1.00 g, 3.57 mmol), styrene (1.86 g, 17.9 mmol), azobisisobutyronitrile (17.7 mg, 0.108 mmol, 0.5 mol%), and 2.8 mL of anisole were charged into a 10 mL Schlenk flask. The flask was then taken outside the glovebox, the mixture subjected to three freeze-pump-thaw cycles, and subsequently immersed in an oil bath preset at 110 °C. After stirring for 24 h the flask was cooled to room temperature, one drop of the polymer solution was taken to determine the monomer conversion of **M1** (92%) and styrene (85%) by $^1$H NMR integration of the residual vinyl group signals of the monomers relative to the Me group signal of anisole. The reaction mixture was precipitated into methanol. The precipitate was collected by filtration and then redissolved in toluene. The copolymer was recovered by repeated reprecipitation from toluene into hexanes (twice) and dried under vacuum. Yield: 1.60 g (56%). $^1$H NMR (500 MHz, $CDCl_3$): δ = 7.4 - 6.2 (overlapped aromatic protons), 2.52 (broad s, Me), 2.3 - 1.3 (overlapped backbone protons), 0.44 (broad s, $SiMe_3$). GPC-RI: $M_n$ = 18800 g mol$^{-1}$, $M_w$ = 31000 g mol$^{-1}$, $Đ$ = 1.65; $X(\boldsymbol{M1})_{n\ GPC}$ = 24, $X(St)_{n\ GPC}$ = 116. The product contains 18 mol% Si monomer based on $^1$H NMR integration of the $SiMe_3$ signal relative to aromatic signals (17 mol% based on the feed ratio).

**Conversion to Poly((3,5-dimethyl-4'-vinyl-[1,1'-biphenyl]-4-yl)bis(pentafluorophenyl)-borane)-co-Polystyrene (P1-BPf2).** In a glovebox, **P1-Si** (250.0 mg, 0.327 mmol $SiMe_3$ groups) was dissolved in toluene (3 mL). A solution of $BBr_3$ (90.1 mg, 0.360 mmol) in 0.2 mL of toluene

was added dropwise, and the mixture was allowed to stir at room temperature for 12 h. The formation of the dibromoborylated intermediate was confirmed by $^{1}H$ and $^{11}B$ NMR spectroscopy of the crude mixture: $^{1}H$ NMR (500.0 MHz, $CDCl_3$): δ = 7.2 - 6.3 (overlapped aromatic protons), 2.39 (broad s, Me), 2.2 - 1.3 (overlapped backbone protons); $^{11}B$ NMR (160.4 MHz, $CDCl_3$): δ = 59.6. The polymer mixture was diluted with 10 mL toluene, then, a solution of $Zn(C_6F_5)_2$ (195.6 mg, 0.490 mmol) in toluene (0.1 mL) was added dropwise at room temperature. The mixture was kept stirring at 80 °C for 48 h. A solid precipitate formed and was removed by filtration through a small pad of celite. The solvent was removed under high vacuum. Purification by reprecipitation from toluene into hexanes (three times) and drying under high vacuum gave the product as a light yellow fluorescent solid. Yield: 0.218 g (64%). $^{1}H$ NMR (500 MHz, $CDCl_3$): δ = 7.4 – 6.2 (overlapped aromatic protons), 2.17 (broad s, Me), 2.0 – 1.3 (overlapped backbone protons). $^{19}F$ NMR (470.3 MHz, $CDCl_3$): δ = -128.3 (4n F, Pf), -145.0 (2n F, Pf), -160.4 (4n F, Pf). $^{11}B$ NMR (160.4 MHz, $CDCl_3$): δ = 68 (very broad).

**Synthesis of Poly((3-chloro-4'-vinyl-[1,1'-biphenyl]-4-yl)trimethylsilane)-co-PS (P2-Si).** In a glovebox, monomer **M2** (1.00 g, 3.49 mmol), styrene (1.81 g, 17.4 mmol), azobisisobutyronitrile (17.2 mg, 0.105 mmol, 0.5 mol%), and 2.8 mL of anisole were charged into a 10 mL Schlenk flask. The flask was then taken outside the glovebox, the mixture subjected to three freeze-pump-thaw cycles, and subsequently immersed in an oil bath preset at 110 °C. After stirring for 24 h the flask was cooled to room temperature and one drop of the polymer solution was taken to determine the monomer conversion of **M2** (75%) and styrene (68%) by $^{1}H$ NMR integration of the residual vinyl group signals of the monomers relative to the Me group signal of anisole. The reaction mixture was precipitated into methanol. The precipitate was collected by filtration and then redissolved in toluene. The copolymer was recovered by repeated reprecipitation from toluene into hexanes

(twice) and dried under high vacuum. Yield: 1.72 g (61%). $^{1}$H NMR (500 MHz, $CDCl_3$): δ = 7.6 – 7.3 (aromatic protons of functional monomer), 7.3 – 6.2 (overlapped aromatic protons), 2.3 – 1.2 (overlapped backbone protons), 0.45 (broad s, $SiMe_3$). GPC-RI: $M_n$ = 39300 g mol$^{-1}$, $M_w$ = 82400 g mol$^{-1}$, $Đ$ = 2.09; $X(M2)_{n\ GPC}$ = 53, $X(St)_{n\ GPC}$ = 230. The product contains 13 mol% Si monomer based on $^{1}$H NMR integration of the $SiMe_3$ signal relative to the aromatic signals (17 mol% based on the feed ratio).

**Conversion to Poly((3-chloro-4'-vinyl-[1,1'-biphenyl]-4-yl)bis(pentafluoro-phenyl)borane)-co-PS (P2-BPf2).** In a glovebox, **P2-Si** (500.0 mg, 0.492 mmol $SiMe_3$ groups) was dissolved in toluene (3 mL), followed by dropwise addition of a solution of $BBr_3$ (0.370 g, 1.48 mmol) in toluene (0.2 mL). The mixture was allowed to stir at 80 ºC for 24 h. The formation of the dibromoborylated intermediate was confirmed by $^{1}$H and $^{11}$B NMR spectroscopy. $^{1}$H NMR (500.0 MHz, $CDCl_3$): δ = 7.6 – 7.4 (aromatic protons of borane monomer), 7.2 – 6.4 (overlapped aromatic protons), 2.5 – 1.3 (overlapped backbone protons); $^{11}$B NMR (160.4 MHz, $CDCl_3$): δ = 55.1. The polymer was precipitated into dry hexanes to remove the excess of $BBr_3$. The precipitate was redissolved in toluene (20 mL), a solution of $Zn(C_6F_5)_2$ (0.206 g, 0.516 mmol) in toluene (5 mL) was added dropwise, and stirring was continued at room temperature for 24 h. A white precipitate formed that was removed by filtration through a small pad of celite. The solvent was evaporated under high vacuum. Purification by repeated reprecipitation from toluene into hexanes (three times) and drying under high vacuum gave the product as a light yellow solid. Yield: 0.350 g (56%). $^{1}$H NMR (500 MHz, $CDCl_3$): δ = 7.7 – 7.4 (aromatic protons of borane monomer), 7.3 – 6.2 (overlapped aromatic protons), 2.3 – 1.2 (overlapped backbone protons). $^{19}$F NMR (470.3 MHz, $CDCl_3$): δ = -128.0 (4n F, Pf), -146.2 (2n F, Pf), -160.6 (4n F, Pf). $^{11}$B NMR (160.4 MHz, $CDCl_3$): δ = 62.9.

**Acknowledgments**

This material is based upon work supported by the National Science Foundation under Grants CHE-1609043 and CHE-1904791. The Bruker 500 MHz NMR spectrometer used in this study was acquired with partial support by an NSF-MRI grant (CHE-1229030). Equipment in the Polymer and Nanomaterials Facility at Rutgers University Newark was acquired with support by the New Jersey Higher Education Equipment Leasing Fund (ELF III 047-04). We thank Professor Piotrowiak for support with low temperature measurements.

**Supporting Information.** Synthetic procedures and characterization details for precursors, monomers and model compounds, multinuclear NMR and mass spectra for monomers and model compounds, multinuclear NMR spectra and GPC traces for polymers, $^{11}B$ and $^{19}F$ NMR data related to stability studies in wet solvents, $^{1}H$ NMR data related to catalysis studies, absorption and emission data in solvents of varying polarity, time-resolved fluorescence and phosphorescence decay curves and fits, comparisons of prompt and delayed emission spectral data of polymers and model compounds at RT and 77 K, comparison of experimentally and computationally determined singlet and triplet energy levels, cyclic voltammograms of model compounds, results of DFT and TD-DFT calculations including depictions of optimized geometries, frontier orbitals, and cartesian coordinates.

## References


1. Ji, L.; Griesbeck, S.; Marder, T. B., Recent Developments in and Perspectives on Three-Coordinate Boron Materials: A Bright Future. *Chem. Sci.* **2017**, *8*, 846-863.

2. Mellerup, S. K.; Wang, S., Boron-Doped Molecules for Optoelectronics. *Trends Chem.* **2019**, *1*, 77-89.

3. Huo, J.; Wang, H.; Li, S.; Shi, H.; Tang, Y.; Tang, B. Z., Design and Development of Highly Efficient Light‐Emitting Layers in OLEDs with Dimesitylboranes: An Updated Review. *Chem. Rec.* **2020**, *20*, 556-569.

4. Stephan, D. W., The broadening reach of frustrated Lewis pair chemistry. *Science* **2016**, *354*, aaf7229.

5. Jupp, A. R.; Stephan, D. W., New Directions for Frustrated Lewis Pair Chemistry. *Trends Chem.* **2019**, *1*, 35-48.

6. Stephan, D. W.; Erker, G., Frustrated Lewis Pairs: Metal-free Hydrogen Activation and More. *Angew. Chem. Int. Ed.* **2010**, *49*, 46-76.

7. Mahdi, T.; Stephan, D. W., Frustrated Lewis Pair Catalyzed Hydroamination of Terminal Alkynes. *Angew. Chem. Int. Ed.* **2013**, *52*, 12418-12421.

8. Courtemanche, M.-A.; Légaré, M.-A.; Maron, L.; Fontaine, F.-G., A Highly Active Phosphine–Borane Organocatalyst for the Reduction of CO2 to Methanol Using Hydroboranes. *J. Am. Chem. Soc.* **2013**, *135*, 9326-9329.

9. Parks, D. J.; Piers, W. E., Tris(pentafluorophenyl)boron-catalyzed hydrosilation of aromatic aldehydes, ketones, and esters. *J. Am. Chem. Soc.* **1996**, *118*, 9440-9441.

10. Rubin, M.; Schwier, T.; Gevorgyan, V., Highly Efficient B(C6F5)3-Catalyzed Hydrosilylation of Olefins. *J. Org. Chem.* **2002**, *67*, 1936-1940.

11. Rendler, S.; Oestreich, M., Conclusive evidence for an S(N)2-Si mechanism in the B(C(6)F(5))(3)-catalyzed hydrosilylation of carbonyl compounds: Implications for the related hydrogenation. *Angew. Chem. Int. Ed.* **2008**, *47*, 5997-6000.

12. Houghton, A. Y.; Hurmalainen, J.; Mansikkamaki, A.; Piers, W. E.; Tuononen, H. M., Direct observation of a borane-silane complex involved in frustrated Lewis-pair-mediated hydrosilylations. *Nat. Chem.* **2014**, *6*, 983-988.

13. Itsuno, S., Polymer-Supported Metal Lewis Acids. In *Lewis Acids in Organic Synthesis*, Yamamoto, H., Ed. Wiley VCH: Weinheim, New York, Chichester, Brisbane, Singapore, Toronto, 2000; Vol. 2, pp 945-979.

14. Jäkle, F., Lewis acidic organoboron polymers. *Coord. Chem. Rev.* **2006**, *250*, 1107-1121.

15. Vidal, F.; Jäkle, F., Functional Polymeric Materials Based on Main-Group Elements. *Angew. Chem. Int. Ed.* **2019**, *58*, 5846-5870.

16. Jäkle, F., Borylated Polystyrenes as Versatile Functional Materials. In *New Polymeric Materials Based on Element-Blocks*, Chujo, Y., Ed. Springer Singapore: Singapore, 2019; pp 59-76.

17. Matsumi, N.; Chujo, Y., pi-conjugated organoboron polymers via the vacant p-orbital of the boron atom. *Polym. J.* **2008**, *40*, 77-89.

18. Jäkle, F., Advances in the Synthesis of Organoborane Polymers for Optical, Electronic and Sensory Applications. *Chem. Rev.* **2010**, *110*, 3985-4022.

19. Nagai, A.; Chujo, Y., Luminescent Organoboron Conjugated Polymers. *Chem. Lett.* **2010**, *39*, 430-435.

20. Tanaka, K.; Chujo, Y., Advanced Luminescent Materials Based on Organoboron Polymers. *Macromol. Rapid Comm.* **2012**, *33*, 1235-1255.

21. Polgar, A. M.; Poisson, J.; Paisley, N. R.; Christopherson, C. J.; Reyes, A. C.; Hudson, Z. M., Blue to Yellow Thermally Activated Delayed Fluorescence with Quantum Yields near Unity in Acrylic Polymers Based on D– π –A Pyrimidines. *Macromolecules* **2020**, *53*, 2039-2050.

22. Qin, Y.; Cheng, G.; Sundararaman, A.; Jäkle, F., Well-Defined Boron-Containing Polymeric Lewis Acids. *J. Am. Chem. Soc.* **2002**, *124*, 12672-12673.

23. Qin, Y.; Cheng, G.; Achara, O.; Parab, K.; Jäkle, F., A New Route to Organoboron Polymers via Highly Selective Polymer Modification Reactions. *Macromolecules* **2004**, *37*, 7123-7131.

24. Parab, K.; Venkatasubbaiah, K.; Jäkle, F., Luminescent Triarylborane-Functionalized Polystyrene: Synthesis, Photophysical Characterization, and Anion Binding Studies. *J. Am. Chem. Soc.* **2006**, *128*, 12879-12885.

25. Parab, K.; Doshi, A.; Cheng, F.; Jäkle, F., Synthesis and Characterization of Luminescent Polystyrene Derivatives with Sterically Protected Fluorenyl- and Carbazolylborane Moieties. *Macromolecules* **2011**, *44*, 5961-5967.

26. Sung, W. Y.; Park, M. H.; Park, J. H.; Eo, M.; Yu, M. S.; Do, Y.; Lee, M. H., Triarylborane-functionalized polynorbornenes: Direct polymerization and signal amplification in fluoride sensing. *Polymer* **2012**, *53*, 1857-1863.

27. Adams, I. A.; Rupar, P. A., A Poly(9-Borafluorene) Homopolymer: An Electron-Deficient Polyfluorene with "Turn-On" Fluorescence Sensing of NH3 Vapor. *Macromol Rapid Comm* **2015**, *36*, 1336-1340.

28. Cheng, F.; Bonder, E. M.; Jäkle, F., Electron-Deficient Triarylborane Block Copolymers: Synthesis by Controlled Free Radical Polymerization and Application in the Detection of Fluoride Ions. *J. Am. Chem. Soc.* **2013**, *135*, 17286-17289.

29. Wang, M.; Nudelman, F.; Matthes, R. R.; Shaver, M. P., Frustrated Lewis Pair Polymers as Responsive Self-Healing Gels. *J. Am. Chem. Soc.* **2017**, *139*, 14232-14236.

30. Yolsal, U.; Wang, M.; Royer, J. R.; Shaver, M. P., Rheological Characterization of Polymeric Frustrated Lewis Pair Networks. *Macromolecules* **2019**, *52*, 3417-3425.

31. Vidal, F.; Lin, H.; Morales, C.; Jäkle, F., Polysiloxane/Polystyrene Thermo-Responsive and Self-Healing Polymer Network via Lewis Acid-Lewis Base Pair Formation. *Molecules* **2018**, *23*, 405.

32. Vidal, F.; Gomezcoello, J.; Lalancette, R. A.; Jäkle, F., Lewis Pairs as Highly Tunable Dynamic Cross-Links in Transient Polymer Networks. *J. Am. Chem. Soc.* **2019**, *141*, 15963-15971.

33. Trunk, M.; Teichert, J. F.; Thomas, A., Room-Temperature Activation of Hydrogen by Semi-immobilized Frustrated Lewis Pairs in Microporous Polymer Networks. *J. Am. Chem. Soc.* **2017**, *139*, 3615-3618.

34. Willms, A.; Schumacher, H.; Tabassum, T.; Qi, L.; Scott, S. L.; Hausoul, P. J. C.; Rose, M., Solid Molecular Frustrated Lewis Pairs in a Polyamine Organic Framework for the Catalytic Metal-free Hydrogenation of Alkenes. *Chemcatchem* **2018**, *10*, 1835-1843.

35. Ma, Y. Y.; Zhang, S.; Chang, C. R.; Huang, Z. Q.; Ho, J. C.; Qu, Y. Q., Semi-solid and solid frustrated Lewis pair catalysts. *Chem. Soc. Rev.* **2018**, *47*, 5541-5553.

36. Chen, L.; Liu, R.; Yan, Q., Polymer Meets Frustrated Lewis Pair: Second-Generation CO2-Responsive Nanosystem for Sustainable CO2 Conversion. *Angew. Chem. Int. Ed.* **2018**, *57*, 9336-9340.

37. Eros, G.; Mehdi, H.; Papai, I.; Rokob, T. A.; Kiraly, P.; Tarkanyi, G.; Soos, T., Expanding the Scope of Metal-Free Catalytic Hydrogenation through Frustrated Lewis Pair Design. *Angew. Chem. Int. Ed.* **2010**, *49*, 6559-6563.

38. Gyömöre, Á.; Bakos, M.; Földes, T.; Pápai, I.; Domján, A.; Soós, T., Moisture-Tolerant Frustrated Lewis Pair Catalyst for Hydrogenation of Aldehydes and Ketones. *Acs Catal.* **2015**, *5*, 5366-5372.

39. Dorkó, É.; Szabó, M.; Kótai, B.; Pápai, I.; Domján, A.; Soós, T., Expanding the Boundaries of Water-Tolerant Frustrated Lewis Pair Hydrogenation: Enhanced Back Strain in the Lewis Acid Enables the Reductive Amination of Carbonyls. *Angew. Chem. Int. Ed.* **2017**, *56*, 9512-9516.

40. Blagg, R. J.; Simmons, T. R.; Hatton, G. R.; Courtney, J. M.; Bennett, E. L.; Lawrence, E. J.; Wildgoose, G. G., Novel B(Ar ')(2)(Ar '') hetero-tri(aryl)boranes: a systematic study of Lewis acidity. *Dalton Trans.* **2016**, *45*, 6032-6043.

41. Scott, D. J.; Fuchter, M. J.; Ashley, A. E., Designing effective 'frustrated Lewis pair' hydrogenation catalysts. *Chem. Soc. Rev.* **2017**, *46*, 5689-5700.

42. Bergbreiter, D. E.; Tian, J. H.; Hongfa, C., Using Soluble Polymer Supports To Facilitate Homogeneous Catalysis. *Chem. Rev.* **2009**, *109*, 530-582.

43. Lu, J.; Toy, P. H., Organic Polymer Supports for Synthesis and for Reagent and Catalyst Immobilization. *Chem. Rev.* **2009**, *109*, 815-838.

44. Bergbreiter, D. E., Soluble Polymers as Tools in Catalysis. *Acs Macro Lett.* **2014**, *3*, 260-265.

45. Gaffen, J. R.; Bentley, J. N.; Torres, L. C.; Chu, C.; Baumgartner, T.; Caputo, C. B., A Simple and Effective Method of Determining Lewis Acidity by Using Fluorescence. *Chem* **2019**, *5*, 1567-1583.

46. Thompson, B. L.; Simons, C. R.; Heiden, Z. M., Redox switchable catalysis utilizing a fluorescent dye. *Chem. Commun.* **2019**, *55*, 11430-11433.

47. Iwama, N.; Tayano, T.; Ohtaki, H. Catalyst component for olefin polymerization, catalyst for α-olefin polymerization and process for the production of α-olefin polymer. US20050070426A1, 2005.

48. Beckett, M. A.; Strickland, G. C.; Holland, J. R.; Sukumar Varma, K., A convenient n.m.r. method for the measurement of Lewis acidity at boron centres: correlation of reaction rates of Lewis acid initiated epoxide polymerizations with Lewis acidity. *Polymer* **1996**, *37*, 4629-4631.

49. Noda, T.; Shirota, Y., 5,5‘-Bis(dimesitylboryl)-2,2‘-bithiophene and 5,5‘‘-Bis(dimesitylboryl)-2,2‘:5‘,2‘‘-terthiophene as a Novel Family of Electron-Transporting Amorphous Molecular Materials. *J. Am. Chem. Soc.* **1998**, *120*, 9714-9715.

50. Hatakeyama, T.; Shiren, K.; Nakajima, K.; Nomura, S.; Nakatsuka, S.; Kinoshita, K.; Ni, J.; Ono, Y.; Ikuta, T., Ultrapure Blue Thermally Activated Delayed Fluorescence Molecules: Efficient HOMO–LUMO Separation by the Multiple Resonance Effect. *Adv. Mater.* **2016**, *28*, 2777-2781.

51. Zhang, M.-Y.; Li, Z.-Y.; Lu, B.; Wang, Y.; Ma, Y.-D.; Zhao, C.-H., Solid-State Emissive Triarylborane-Based [2.2]Paracyclophanes Displaying Circularly Polarized Luminescence and Thermally Activated Delayed Fluorescence. *Org. Lett.* **2018**, *20*, 6868-6871.

52. Pagidi, S.; Kalluvettukuzhy, N. K.; Thilagar, P., Effect of Branching on the Delayed Fluorescence and Phosphorescence of Simple Borylated Arylamines. *Inorg. Chem.* **2020**, *59*, 3142-3151.

53. Ma, J.-L.; Liu, H.; Li, S.-Y.; Li, Z.-Y.; Zhang, H.-Y.; Wang, Y.; Zhao, C.-H., Metal-Free Room-Temperature Phosphorescence from Amorphous Triarylborane-Based Biphenyl. *Organometallics* **2020**, *DOI: 10.1021/acs.organomet.0c00068*.

54. Wu, Z.; Nitsch, J.; Schuster, J.; Friedrich, A.; Edkins, K.; Loebnitz, M.; Dinkelbach, F.; Stepanenko, V.; Würthner, F.; Marian, C. M.; Ji, L.; Marder, T. B., Persistent Room Temperature Phosphorescence from Triarylboranes: A Combined Experimental and Theoretical Study. *Angew. Chem. Int. Ed.* **2020**, *59*, 17137-17144.

55. Zhang, Z.; Edkins, R. M.; Nitsch, J.; Fucke, K.; Steffen, A.; Longobardi, L. E.; Stephan, D. W.; Lambert, C.; Marder, T. B., Optical and electronic properties of air-stable organoboron compounds with strongly electron-accepting bis(fluoromesityl)boryl groups. *Chem. Sci.* **2015**, *6*, 308-321.

56. Sun, Z.-B.; Liu, J.-K.; Yuan, D.-F.; Zhao, Z.-H.; Zhu, X.-Z.; Liu, D.-H.; Peng, Q.; Zhao, C.-H., 2,2′-Diamino-6,6′-diboryl-1,1′-binaphthyl: A Versatile Building Block for Temperature-Dependent Dual Fluorescence and Switchable Circularly Polarized Luminescence. *Angew. Chem. Int. Ed.* **2019**, *58*, 4840-4846.

57. Wang, C.; Xu, Q.-W.; Zhang, W.-N.; Peng, Q.; Zhao, C.-H., Charge-Transfer Emission in Organoboron-Based Biphenyls: Effect of Substitution Position and Conformation. *J. Org. Chem.* **2015**, *80*, 10914-10924.

58. Uoyama, H.; Goushi, K.; Shizu, K.; Nomura, H.; Adachi, C., Highly efficient organic light-emitting diodes from delayed fluorescence. *Nature* **2012**, *492*, 234–238.

59. Belaidi, H.; Rauch, F.; Zhang, Z.; Latouche, C.; Boucekkine, A.; Marder, T. B.; Halet, J.-F., Insights into the Optical Properties of Triarylboranes with Strongly Electron-Accepting Bis(fluoromesityl)boryl Groups: when Theory Meets Experiment. *ChemPhotoChem* **2020**, *4*, 173-180.

60. Cummings, S. A.; Iimura, M.; Harlan, C. J.; Kwaan, R. J.; Trieu, I. V.; Norton, J. R.; Bridgewater, B. M.; Jäkle, F.; Sundararaman, A.; Tilset, M., An estimate of the reduction potential of B(C6F5)(3) from electrochemical measurements on related mesityl boranes. *Organometallics* **2006**, *25*, 1565-1568.

61. The transition energy is slightly overestimated as is frequently observed when using the cam-b3lyp hybrid exchange-correlation functional that is based on the coulomb-attenuating method. Similar calculations with the b3lyp functional significantly underestimate the transition energies (SI). See: Makarov, N. S.; Mukhopadhyay, S.; Yesudas, K.; Brédas, J.-L.; Perry, J. W.; Pron, A.; Kivala, M.; Müllen, K., Impact of Electronic Coupling, Symmetry, and Planarization on One- and Two-Photon Properties of Triarylamines with One, Two, or Three Diarylboryl Acceptors. *J. Phys. Chem. A* **2012**, *116*, 3781-3793.